Electrochimica Acta 71 (2012) 258–265

Contents lists available at SciVerse ScienceDirect

Electrochimica Acta

journal homepage: www.elsevier.com/locate/electacta

A comprehensive understanding of electrode thickness effects on the electrochemical performances of Li-ion battery cathodes

Honghe Zheng[a,b,*], Jing Li[a], Xiangyun Song[b], Gao Liu[b], Vincent S. Battaglia[b]

[a] School of Energy, Soochow University, Suzhou, Jiangsu 215006, PR China
[b] Lawrence Berkeley National Laboratory, 1 Cyclotron Rd., Berkeley, CA 94720, USA

ARTICLE INFO

Article history:
Received 31 December 2011
Received in revised form 25 March 2012
Accepted 31 March 2012
Available online 6 April 2012

Keywords:
Lithium ion batteries
Electrode thickness
Rate capability
Energy density
Power density

ABSTRACT

$LiNi_{1/3}Co_{1/3}Mn_{1/3}O_2$ (NCM) and $LiFePO_4$ (LFP) electrodes of different active material loadings are prepared. The impact of electrode thickness on the rate capability, energy and power density and long-term cycling behavior is comparatively investigated. Peukert coefficient slightly increases with increasing electrode thickness, showing a severe capacity loss at higher rate for thicker electrode. A power-law relation between the maximum working *C* rate and electrode loading is obtained. Increase of the specific resistance with increasing electrode thickness is not an important factor responsible for the poor rate performance for thicker electrode. The power–law relationship is typical for a diffusion-related system, indicating that Li ion diffusion within the electrode is the rate-determining step for the discharge process. As the result of the deterioration of rate capability, enhancing energy density through increasing electrode thickness is accompanied by a significant loss of power density. Long-term cycling performance is also deteriorated, which is attributed to the high internal resistance and poor mechanical integrity of thicker electrode.

1. Introduction

Lithium-ion batteries (LIBs) are very promising for powering electric vehicles (EVs) and plug-in hybrid electric vehicles (PHEVs). However, there are still many competing cell chemistries and cell designs with varying capabilities for these applications. So far, much effort has been made in fabricating and optimizing different electrode active materials. Studies on electrode structural analysis are reaching a very high level of precision by using different modern spectroscopic techniques; however, it must be kept in mind that engineering issues are just as important as finding new materials or other optimization and modification methodologies such as heat-treating, doping, and surface coating [1–4]. Therefore, more attention need to be paid to identify major factors responsible for the technical barriers limiting the development of advanced Li-ion batteries for automobile applications and to discover the possible scientific issues involved in key technologies.

Specific energy and specific power per weight and per volume requirements are the huge challenges among many of the aggressive requirements for lithium ion batteries for PHEV purposes. In electrode design, electrode thickness (active material loading), electrode porosity and chemical composition are important parameters affecting the energy and power capability of the cell. For a given active material, energy density of the electrode could be improved by engineering approaches including increasing electrode thickness, reducing electrode porosity and decreasing the content of inactive materials (polymeric binder and conductive carbon). Optimization of electrode porosity has been theoretically and experimentally discussed in previous studies [5–7], in which optimized porosities of 10–40% are specified according to the electrode chemical composition. Chemical composition also considerably influences the overall electrochemical performances of lithium ion battery cathodes [8–10]. We reported an optimized Polyvinylidene difluoride (PVDF) to acetylene black (AB) ratio of 5:3 for $LiNi_{0.8}Co_{0.15}A_{l0.05}O_2$ (NCA) cathode, at which volumetric energy density of the electrode could be improve by using less inactive materials without loss of power density [11]. Besides these factors, electrode thickness has a significant impact on the energy density of an electrode for using thicker electrode can reduce the fraction of inactive material such as current collector and separator. Argonne National Laboratory attempted to develop high energy density electrode by using thicker electrodes in order to meet the aggressive energy density goal of PHEV batteries [12,13]. In addition, different models based on porous electrode theory have been developed by taking into several important physical parameters of batteries to simulate the charge-discharge characteristics [14–16]. Qualitative analyses have been presented to find the relationship between the design variables and electrochemical performance for various battery systems. Although electrode thickness is well

* Corresponding author at: School of Energy, Soochow University, Suzhou, Jiangsu 215006, PR China.
E-mail addresses: hhzheng66@yahoo.com.cn, hhzheng@suda.edu.cn (H. Zheng).

0013-4686/$ – see front matter © 2012 Elsevier Ltd. All rights reserved.
http://dx.doi.org/10.1016/j.electacta.2012.03.161

known as an important design parameter greatly affecting the electrochemical performance of a cell, detailed and quantitative experimental results relating to the electrode thickness effects are not enough, and sometimes even not available. The reported studies have not fully explained the effect of lithium ion diffusion within electrodes due to the difficulty and complexity of a transport process. Some fundamental scientific issues and general laws relating to electrode thickness effects remain a matter of conjecture. A comprehensive understanding of electrode thickness effects is of great significance for designing high quality electrode to meet the EV and PHEV requirements.

This paper presents a comparative study of the impact of electrode thickness on electrochemical performances between $LiNi_{1/3}Co_{1/3}Mn_{1/3}O_2$ (NCM) and $LiFePO_4$ (LFP) cathodes. NCM is employed in this study as it offers high energy and power density compared with other commercial oxide cathode materials [17,18]. By contrast, LFP has advantages of good safety attribute and long cycle life [19,20]. Both the two kinds of cathode materials are widely accepted to be promising for EV and PHEV applications. In this work, the cathode laminates of various thicknesses were prepared with the same chemical composition. The effects of electrode thickness on the rate capability for NCM and LFP electrodes were examined. A power-law relation between maximum working C rate and electrode loadings was developed. Long-term cycling performances for the two cathodes at different thicknesses against a graphite anode were compared. Factors affecting the rate capability and long-term cycling performance of the cathodes were discussed and elucidated.

2. Experimental

NCM sample adopted in this study with a mean particle size of 6–8 μm was supplied by Seimi, USA. The surface area of the material is 0.4$m^2\,g^{-1}$, as determined by the Brunauer–Emmett–Teller (BET) method. The LFP sample was synthesized by a hydrothermal method with an average particle size of 200–300 nm and 3 wt% carbon coating on the particle surface. The surface area was determined to be 15.4 $m^2\,g^{-1}$. Acetylene black (AB) with an average particle size of 40 nm was acquired from Denka Singapore Private Ltd. PVDF (KF1100) binder was obtained from Kureha, Japan. N-Methylpyrrolidone (NMP) was purchased from Aldrich chemical company.

To obtain cathode laminate of different thicknesses, NCM slurry was prepared by mixing 85% active material, 8% PVDF binder, and 7% acetylene black in NMP solvent. LFP slurry was prepared by mixing 80.8% active material, 12% PVDF and 7.2% acetylene black in NMP solvent. The recipes adopted in this study are obtained in our lab as described in the literature [11] for making the NCM and LFP electrodes of high electrochemical performances. A mechanical mixing was carried out at 4000 rpm for 2 h. The slurry was then coated onto Al foil of 28 μm thickness by using a doctor blade. NCM and LFP cathodes of different thicknesses were prepared by varying the doctor blade height. The electrodes were dried at 80 °C and pressed down to ca. 35% porosity with a calender for all the electrode laminates. Physical information for the NCM and LFP cathodes at different thicknesses is summarized in Tables 1 and 2, respectively. A Hitachi S-4700 scanning electron microscope (SEM) operating at 200 kV was used to view the morphologies of the cathodes.

Once calendered, the electrodes were punched into discs of ½ inch diameter (area of 1.27 cm^2) and thoroughly dried for 16 h at 120 °C under vacuum. Three electrode half-cells were assembled by using swagelok cell in which lithium foil was used as both counter electrode and reference electrode. The separator employed was Celgard 2400. The electrolyte was 1 M $LiPF_6$/ethylene carbonate (EC) + diethyl carbonate (DEC) (1:1 by weight ratio) obtained from Novolyte. All the cells were tested using a Maccor Battery Test Cycler at 303 K in a Thermotron Environmental Chamber. Three formation cycles at *C*/10 charge and discharge were applied. The upper cutoff voltage was set at 4.5 V for NCM and at 4.1 V for LFP cathode while the discharge voltage was set at 3.0 V for NCM and 2.2 V for LFP cathode. The rate performance test consisted of full discharges at rates of *C*/10, *C*/5, *C*/2, 1*C*, 2*C*, 5*C*, 10*C*, 20*C*, and so on. A charge of *C*/10 to its upper voltage limit preceded each discharge. Hybrid pulse power characterization (HPPC) tests were performed following the established procedures from 10% to 90% depth of discharge (DOD). During the HPPC pulse, the cell was pulse discharged at 5.0*C* for 10 s followed by a 60 s rest. It was then subject to 3.75C regen pulse for 10 s, immediately followed by *C*/5 constant current discharge to remove 10% of the cell capacity. The area specific impedance (ASI) and weight specific impedance (WSI) was calculated from the voltage difference before and at the end of the discharge/regen pulses by taking the electrode area and the weight of the active materials into consideration.

Full-cells were assembled with standard 2325 coin cell hardware. A meso-carbon micro-bead (MCMB10-28 from Osaka gas, JP) anode of a series thickness was cast to match the cathode of different thicknesses. The anode consists of 88.8% MCMB, 8% PVDF and 3.2% acetylene black. To avoid Li deposition on the anode, the reversible capacity ratio between anode to cathode was controlled to be around 1.1–1.2. Considering the working potential plateau for the MCMB graphite is ca. 0.1 V vs. Li/Li^+, NCM based full-cells were charged to 4.4 V and discharged to 3.0 V while LFP based full cells were charged to 4.0 V and discharged to 2.2 V. Ten formation cycles for the full cells were performed at *C*/24 to ensure that the cells are well formed. Long-term cycling of all the full cells with different electrode thicknesses was carried out with 1*C* charge and 1*C* discharge for 500 cycles.

3. Results and discussion

Fig. 1 shows the morphologies for both NCM and LFP cathode at different magnifications. For NCM cathode, the active material particle consists of agglomerated primary particles of the active intercalation compounds (called secondary particles). The primary particle size of around 6–8 μm is observed in the image. Acetylene black particles are seen evenly distributed in between active material particles. Some of the nano-carbon particles even went into the pores of the active material. For the LFP cathode, particle size of about 200–300 nm is observed. Although the mixing between nano-particles is very difficult as they easily flocculate due to their large surface area [21], the nano-carbon agglomerates are seen uniformly dispersed within the electrode. From the homogenous dispersion of acetylene black within the cathode, the quality of the two cathode composites prepared in this study is good.

Typical discharge curves for NCM and LFP cathodes at a comparable thickness of around 25 μm (exclusive of Al foil) are displayed in Fig. 2. As expected, the discharge capacity depends strongly on *C* rate. The lowering of discharge curve at higher *C* rate is due to polarization induced by the internal resistance of the cell. When the discharge rate exceeds a certain value, a sudden discharge capacity loss of the electrode is observed, which is mainly contributed by the Li ion diffusion into the electrode. When there is a large gradient of the Li ion concentration for the active material particle during the discharge, the electrode potential will drop greatly to the cut-off potential. It is seen that 10*C* is the maximum working current for the NCM electrode. The electrode is able to deliver ca. 70% of its capacity at this rate. The rate capability of the NCM cathode is well compared to the reported result in literature [22] and in agreement with the results reported in literature [23]. Further increase of *C* rate results in a dramatic drop of the discharge capacity because

Table 1
Physical information for NCM cathodes at different laminate thicknesses.

Initial thickness with Al foil (μm)	Final thickness with al foil (μm)	Electrode laminate thickness (μm)	Active material loading (mg cm^{-2})	Electrode density (including Al) (g cm^{-3})
63	52	24	5.56	2.62
101	78	50	11.48	2.64
129	104	76	17.52	2.65
179	132	104	24.01	2.67

Table 2
Physical information for LFP cathodes at different laminate thicknesses.

Initial thickness with Al foil (μm)	Final thickness with al foil (μm)	Electrode laminate thickness (μm)	Active material loading (mg cm^{-2})	Electrode density (including Al) (g cm^{-3})
44	38	10	1.51	2.376
65	53	25	3.64	2.20
102	78	50	7.31	2.07
144	105	77	11.34	2.015
191	136	108	15.83	1.965

the solid-state diffusion of Li^+ becomes a determining factor controlling the reaction rate. As for the LFP cathode, 20*C* is the maximum working current. The electrode can deliver ca. 70% of its capacity at this rate, which is well compared to the reported results [24,25]. Further increase of *C* rate causes a large capacity loss. By comparison, the LFP cathode exhibits better rate capability compared to the NCM cathode at a similar electrode thickness. This is believed to be ascribed to the very small particle size (200–400 nm) of the LFP used in this study. Although the electrical conductivity of LFP is considerably lower than NCM, decreasing the migration distance (the particle radius) of Li ions is known to be more evident to improve the rate performance of the cathodes [33].

Fig. 3 shows the capacities of NCM and LFP cathodes at different laminate thicknesses obtained from various discharge rates between 0.1*C* and 2.0*C*. The electrode capacities in the regime of rates obey the Peukert law $Q = i^{\boldsymbol{k}} \times t$; where $\boldsymbol{k}$ is the Peukert coefficient and *t* is the nominal discharge time (in hours) for a specific C rate. The Peukert coefficients were obtained in the range from 1.013 to 1.075 for the two kinds of cathodes at various laminate thicknesses. This agrees well with the reported 1.019–1.075 for LFP cathodes obtained under different discharge conditions by Dubbary et al. [26,27]. Thinner electrode has a Peukert coefficient close to 1, meaning the accessible capacity of the electrode is less dependent on the discharge rate. The reliability factors of the fits for the curves of thinner electrodes are superior to 95% while the factors greatly decrease for thicker electrode. Discharge capacity of the thickest NCM cathode at 2*C* rate shows to be well below the value extrapolated from Peukert equation. This is because the electrode reaction is not complete in the discharge and the cutoff voltage is reached prior to the completion of the electrochemical reactions at the surface of the electrodes whereas Peukert equation assumes that all electrode reactions were completed at a given rate. The premature cutoff is resulted from both the polarization effect due to the high internal resistance and Li ion diffusion which will be discussed next.

Rate capability for the two cathodes at different thicknesses over a wide *C* rate range is summarized in Fig. 4. Clearly, rate capability for each cathode is strongly dependent on electrode thickness. All the electrodes, regardless of their thickness, can deliver their full capacity at a small discharge rate of 0.1*C*. With increasing discharge rate, capacity retention of the cathodes at

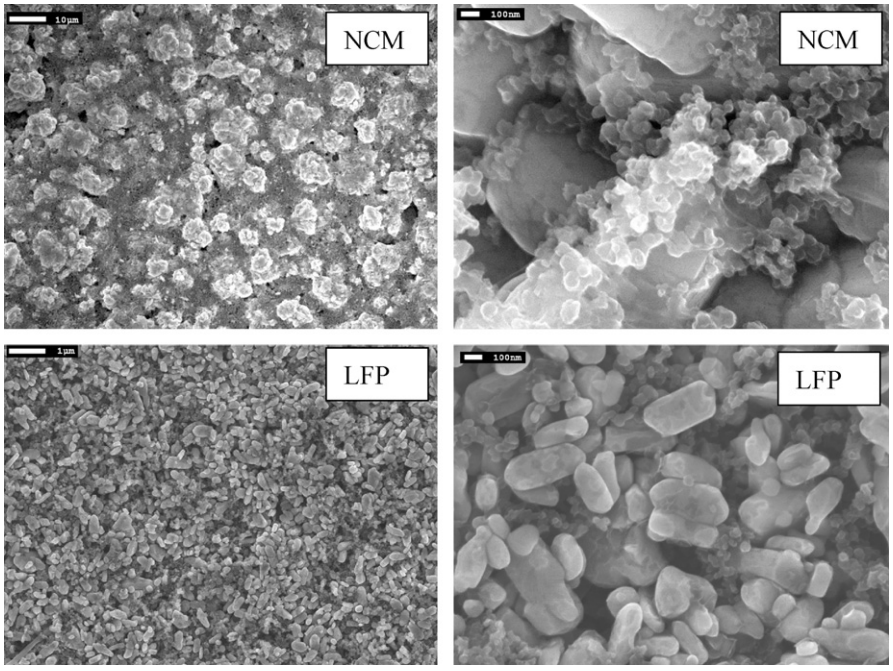

Fig. 1. SEM images of NCM and LFP cathodes at different magnifications.

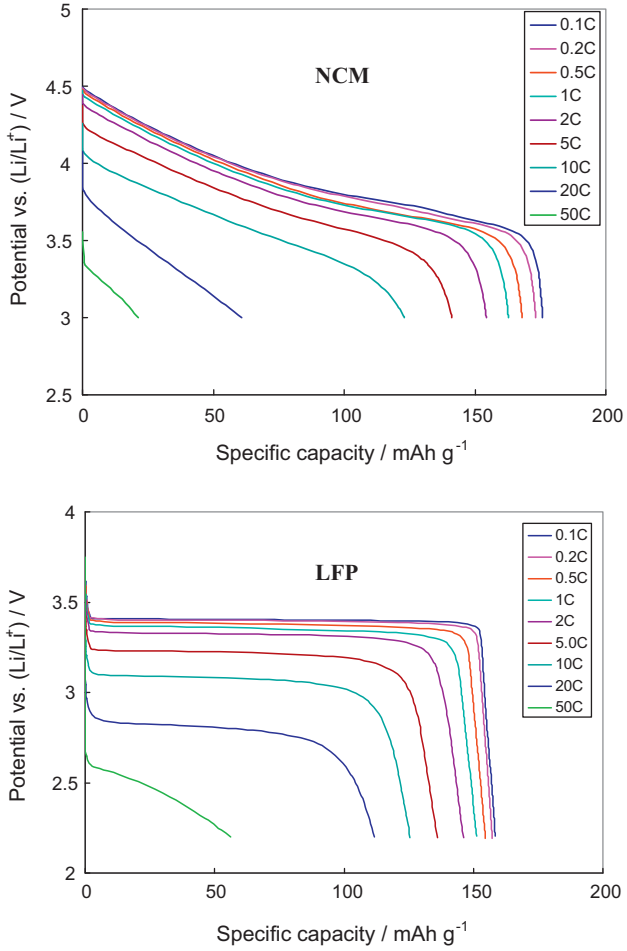

Fig. 2. Discharge profiles of the NCM and LFP cathodes at a comparable thickness of around 25 μm (exclusive of Al foil).

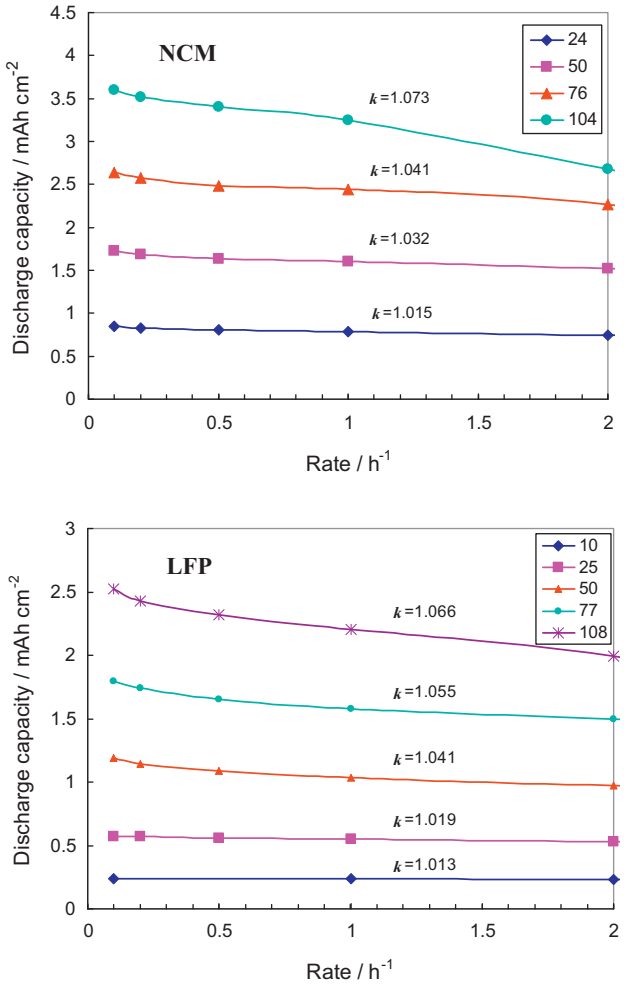

Fig. 3. The Peukert curves for the NCM and LFP cathodes at different electrode thicknesses.

different thicknesses differs significantly. Thinner electrodes can deliver most of its capacity at very high rate while the available capacity dives at a relatively low rate for the thicker one. As shown in this figure, the LFP cathode of 10 μm thickness is capable of discharging at a rate of 100*C* and it still exhibits ca. 70% of its full capacity. By contrast, 2*C* seems to be the maximum operating current for the electrode at 108 μm. This result tells that it is meaningless to compare the rate performance for a material at different electrode thicknesses or active material loadings.

As shown in Fig. 4, each capacity vs. discharge rate curve has an elbow. The point of inflection of the elbow occurs approximately at 70–80% of its full capacity. The discharge rate at the point of inflection, referred to as maximum working *C* rate, can be used to represent the curve and characterize the rate performance of the electrode. The maximum working *C* rate shifts to higher rates for thinner electrodes. Log–log plots between electrode loading (capacity per cm^2) and maximum working *C* rate for both NCM and LFP cathodes are presented in Fig. 5. As electrode thickness (active material loading) increases, the maximum working *C* rate decreases. A power–law relation between electrode loading and the rate performance was obtained. The data points show a linear dependence with a slope of around -0.62 ± 0.05 for both the two cathode materials. The linear relationship between electrode loading and maximum working rate is consistent with the result reported by Yu et al. [28], in which they obtained the $i_{50} * h_0^2 =$ constant, where i_{50} is the operating current corresponding to the 50% capacity retention and h_0 represents the electrode thickness. Of course, active material particle size, electrode composition, electrode architecture, and electrolyte composition may influence the slope and intercept of the line, which needs more detailed studies.

To explain the significant thickness effects on the rate performance of the cathodes, we can consider the electrode as a compound which consists of two continuous phases: the porous solid matrices and liquid electrolyte within the pores. The decrease in capacity of the cathodes at high rates is associated with several different transport processes involved in the electrochemical reaction. These are (1) Electronic resistance of the electrode, R_e; (2) transport of Li ions in the electrolyte to the active material particle surface, R_s; (3) diffusion of Li ions through the solid electrolyte interphase (SEI) film, R_{SEI}; (4) Li-ion charge transfer at the electrode/electrolyte interface, R_{ct}; (5) Li ion diffusion within the bulk electrode, R_{diff}.

The cell polarization (IR drop) is mainly associated the internal resistance, i.e. R_e, R_s, R_{SEI}, and R_{ct} [29]. It is known that $R_e = L/\sigma$, where L is the thickness of the laminate and σ is the electronic conductivity of the electrode laminate. The increase of L definitely contributes to electronic resistance rise of the electrode. In the liquid electrolyte, Li transport between the cathode surface and lithium foil surface is not changed as the thickness and porosity of the separator is the same. The increase of R_s for thicker electrode is resulted from the ionic resistance rise of the electrolyte within the pores of the electrode. Taking the porosity and tortuosity of the electrode into consideration, the increase of Li ion diffusion distance in the liquid phase within the electrode pores

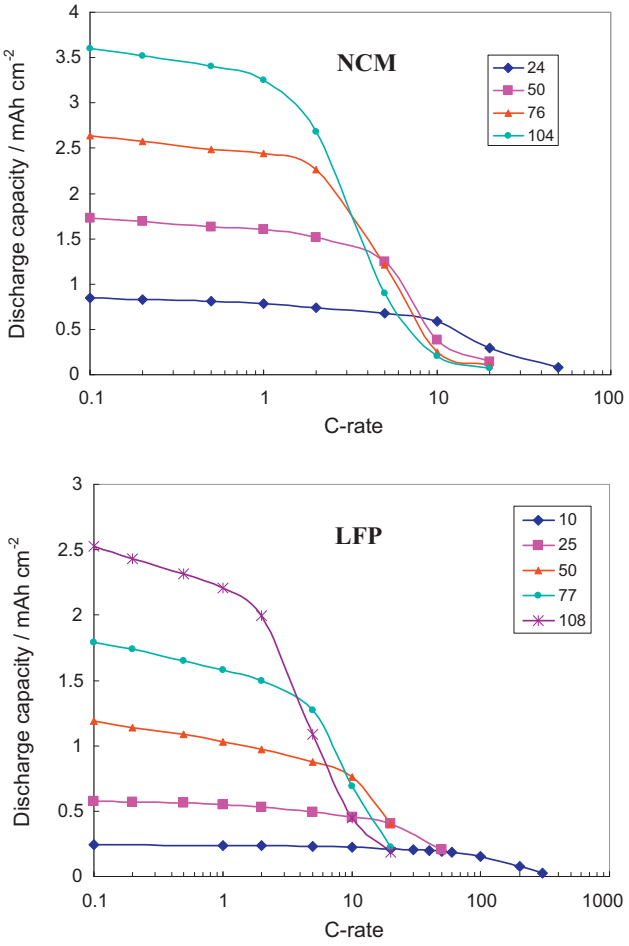

Fig. 4. Discharge capacity as a function of C rate for the NCM and LFP cathodes at different thicknesses.

will be several times larger than the electrode thickness increase. In this sense, the R_s rise with increasing electrode thickness should be quite obvious. R_{SEI} is related to the SEI properties formed on the electrode surface. Since SEI properties are not considerably affected by electrode thickness, the magnitude of R_{SEI} for each cathode at different thicknesses should be relatively stable. R_{ct} evaluates the resistance of Li-ion charge transfer at the electrode/electrolyte

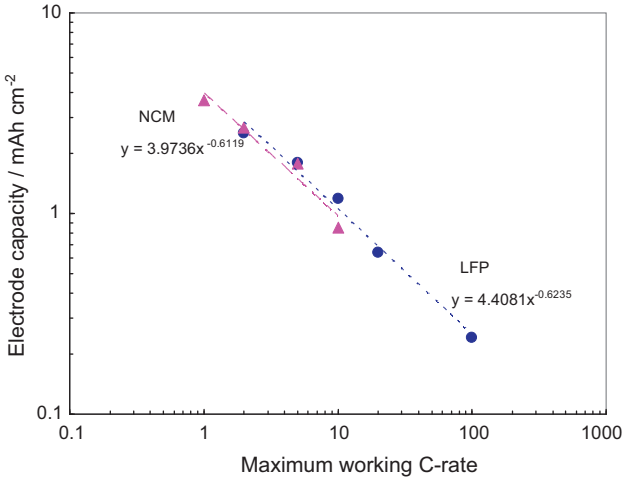

Fig. 5. Log–log plots between the electrode specific capacity and the maximum working *C* rate for the NCM and LFP cathodes.

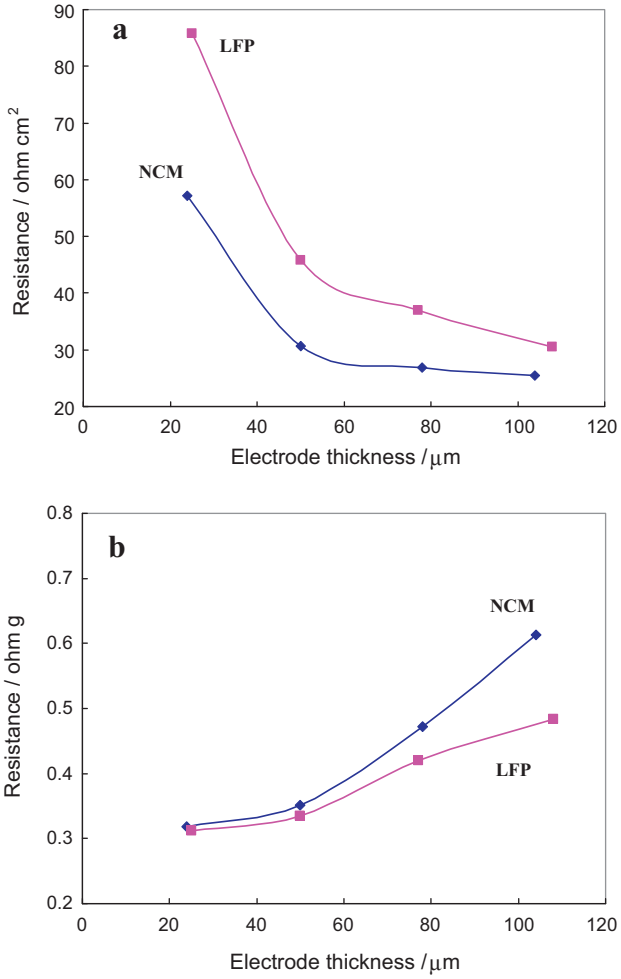

Fig. 6. The area specific impedances (ASI) (a) and weight specific impedance (WSI) (b) at 40% DOD for the NCM and LFP cathodes at different laminate thicknesses.

interface, which mainly determines the internal cell resistance and is known strongly dependent on the electrode potential at a certain temperature. It significantly grows at the end of discharge when Li ion in the bulk electrode is gong to be saturated.

Area specific impedances (ASI) for a cell, reflecting the sum of $R_e + R_s + R_{SEI} + R_{ct}$, can be determined by using HPPC test at different charge or discharge states. ASI calculated for NCM and LFP half cells with various electrode thicknesses at 40% depth of discharge (DOD) are presented in Fig. 6a. ASI for both the two cathodes decreases as the electrode thickness increases. The decreasing trend levels off when the electrode thickness is higher than 60 μm. This is consistent with that reported in the literature [13]. However, the decrease of ASI does not explain the poor rate capability for the thick electrode. Here, it should be noted that the area involved in the ASI calculation is the electrode area, not the specific surface area. For the 1 cm^2 electrode area, the amount of active material is proportional to the electrode thickness. In this sense, the ASI calculated by using electrode area is an extensive property, not an intensive property, which is not comparable between each other.

To solve this problem, the specific impedance of the electrode was re-calculated based on the weight of active material per cm^2 of the electrode, i.e. weight specific impedance (WSI). WSI of the cathodes at different thicknesses are shown in Fig. 6b. This figure shows that the internal resistance shifts to higher value with increasing electrode thickness. This is in agreement with the general belief of lowering the electrode resistance through a thinner coating [30–32]. The internal resistance rise is a reason explaining

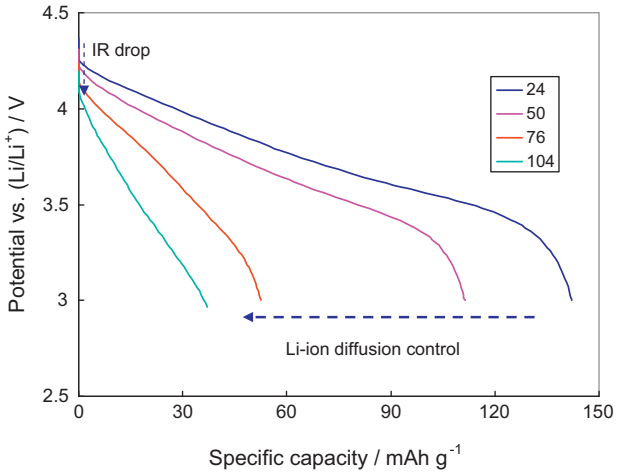

Fig. 7. Comparison of discharge curves for the NCM electrode at the same current density of 5*C*.

the poor power performance of the cathode at higher thicknesses. By the way, WSI of the LFP cathode seems to be slightly lower than that of the NCM. This is due to the extremely high specific area of LFP material than that of the NCM. In this study, 15.4 $m^2\,g^{-1}$ was obtained for LFP material while 0.4 $m^2\,g^{-1}$ was determined for NCM material. Taking the specific area into consideration, the real area specific impedance of LFP will be much higher than that of NCM cathode.

To clearly see the impact of the resistance rise induced by increasing electrode thickness on discharge properties, the discharge curves of the cathodes at different laminate thicknesses are compared at the same current density. Fig. 7 shows a comparison of the discharge curves at 5*C* rate for the NCM electrode at different thicknesses. At the same current density, the onset potential for the discharge reaction was lowered from 4.24 down to 4.06 V due to the internal resistance rise. By contrast, the capacity loss with increasing electrode thickness is not mainly coming from the cell polarization, but from the limitation of Li ion diffusion within the electrode. This is clearly seen for the large capacity loss by increasing electrode thickness from 50 μm to 76 μm, showing that Li ion diffusion is the most important factor deciding the rate performance of the electrode.

The rate controlling factor for Li ion diffusion within the electrode depends on several different physical parameters, including Li ion diffusion coefficient *D*, diffusion length *L*, electrode potential, and position in the electrode, etc. [33–35]. For an electrode of different thicknesses, the kinetics during discharge at any point across the electrode area is as a function of time and space. At a discharge rate as low as *C*/10, the thickness of active layer is less than the characteristic diffusion length and the discharge capacity of the electrode shows to be proportional to the active material loading of the electrode. With increasing C rate, characteristic diffusion length of the electrode is decreased and becomes equal to the electrode thickness at a certain critical rate, i.e. the maximum working *C* rate as we discussed above. Further increase of *C* rate, characteristic diffusion length becomes less than the electrode thickness. In this case, the active material at the electrode surface or even in the bulk electrode becomes electrochemically inert. The observed dramatic capacity loss is because the electrochemical reaction takes place mainly at the electrode surface whereas the electrode surface is no longer electrochemically active at high rates. This phenomenon is qualitatively illustrated by Wang et al. [16] by using one-dimensional model, in which they showed the local current distribution in the solid phase was related to time step and electrode position. According to this simulation, there is a critical thickness

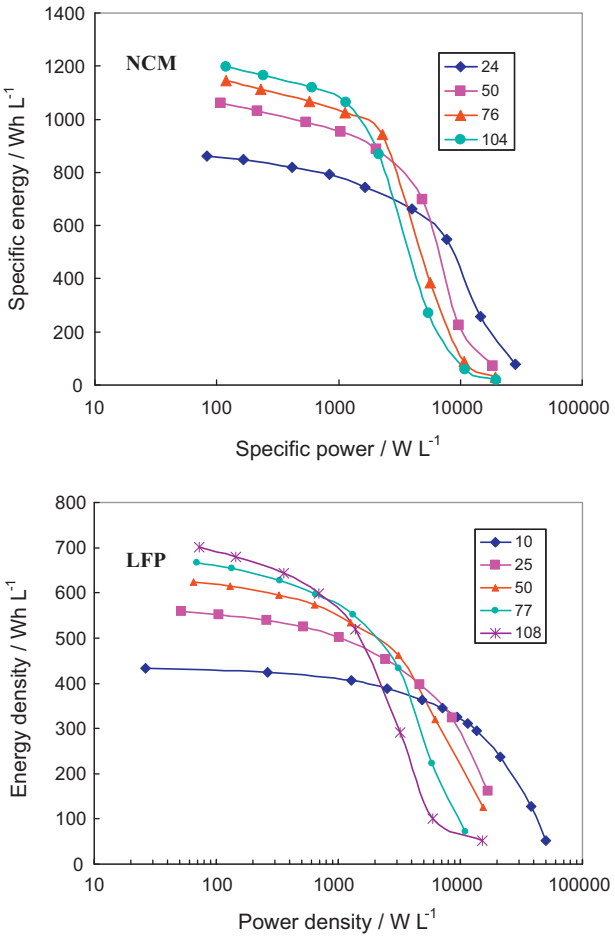

Fig. 8. Ragone plots for the NCM and LFP cathodes at different laminate thicknesses.

for an electrode at a certain *C* rate. This is consistent with the critical working *C* rate we got at each thickness of the cathode in this study. Since the kinetics of the discharge process is very complicated, more sophisticated models need to be developed to quantitatively explain the power–law relationship between electrode loading and the rate capability. For a wide range of crystalline materials, the a.c. impedance in the low frequency regime, which is attributed to the diffusion of lithium ions within the electrode, is described by the well known Jonscher's power–law equation [36]. This is consistent with the power–law relation between the electrode thickness and maximum working *C* rate obtained in this study.

To demonstrate the variation of energy density and power density for the cathodes with respect to cathode thickness, a simple calculation was done taking the Al foil thickness into account. The thickness of the Al current collector was taken to be 14 μm in the calculation as each side is covered with electrode laminate in industry. Fig. 8 is the Ragone plot showing the variations of the energy density for the NCM and LFP cathodes with power density. To clearly see the improvement of energy density by increasing electrode thickness, the plot is shown in semi-log co-ordinate. It is seen the energy density is increasing with electrode thickness. For the NCM cathode, an increase of energy density from 830 Wh L^{-1} (Watt hour per liter) to 1200 Wh L^{-1} is obtained when the laminate thickness is increased from 24 μm to 108 μm. Meanwhile, the electrode energy density of LFP is improved from 550 Wh L^{-1} to 700 Wh L^{-1} from 25 μm to 108 μm thickness. The improvement is attributed to the decrease of Al volume fraction in the electrode. If the other inactive materials such as separator and cell package are considered in the calculation, the improvement of energy

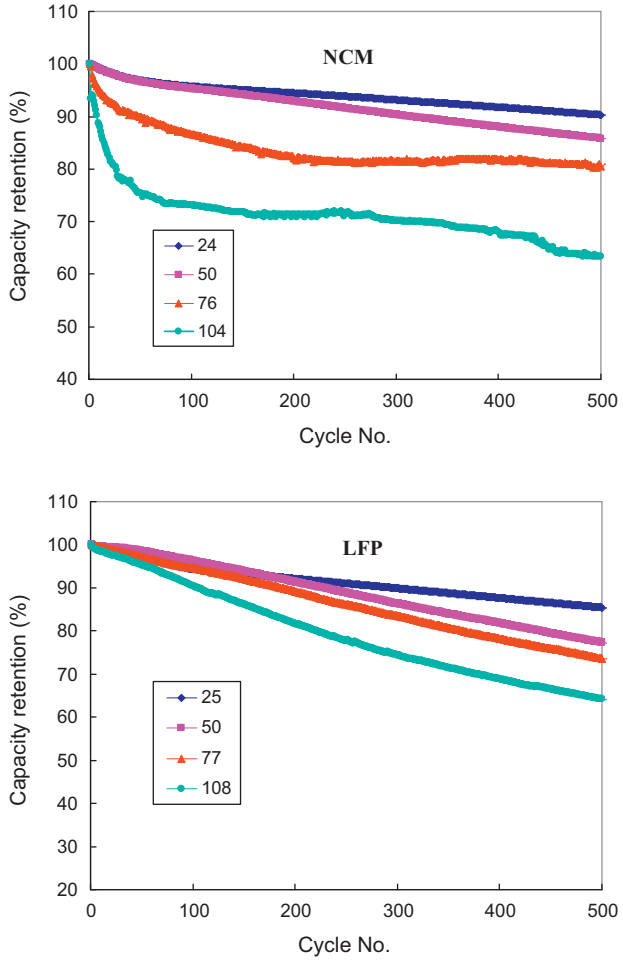

Fig. 9. The normalized capacity retention for lithium ion cells based on the NCM and LFP cathodes at different laminate thicknesses as a function of cycle number.

density will be even more obvious. However, it must be noticed that, with increasing energy density of the electrode, the maximum working power density is greatly decreased. A maximum power is approached for the cathode at each thickness, and the curve bends over and becomes almost vertical at its critical power. Results so far have focused exclusively on energy density as the objective function, since that tends to be the most critical limitation on battery performance in a variety of applications. Power density is also of great significance for EV and PHEV applications. There is a trade-off between energy density and power density through varying electrode thickness. Thick electrode can meet the requirement of high energy density at moderate/low power level. When high current rate are required for high-power applications, the strategy is to decrease the electrode thickness and reduce the energy density.

Long-term cycling behavior of the NCM and LFP cathodes of different thicknesses was tested against MCMB anode. After 10 formation cycles at *C*/24, cycle life of all these full-cells was carried out at 1*C* charge and 1*C* discharge rate. The normalized capacity fading of the cells with various electrode loading as a function of cycle number are displayed in Fig. 9. With the same cathode and anode materials, long term cycling performances of the full cells containing electrode of different thicknesses displayed a clear distinction. An obvious difference in terms of capacity fading-rate with cycle number is observed. For NCM cathode, 24 μm thickness electrode retained 92% of its capacity while 104 μm thickness electrode lost 40% of its capacity after 500 cycles. As for LFP cathode, the thinnest electrode of 10 μm is not subject to full cell cycling because it is hard to make the appropriate anode to match it. After 500 cycles, the electrode of 25 μm thick had a capacity retention of around 90% while more than 30% of its capacity was lost for the electrode of 108 μm thick. Overall, a higher capacity fading-rate is observed for the cell with thicker electrode.

Two factors are considered as the main reasons responsible for the high capacity fading-rate for the cells with thick electrode. One is due to the high internal resistance for the thick electrode as we can see from Fig. 6b. Over-potential aroused from high polarization can induce more side reactions during electrochemical cycles, such as electrolyte oxidation and irreversible phase transformation such as mixing between Li and metal ions and oxygen release for NCM cathode during repeatedly electrochemical cycles [37–39]. The other one reason is believed to be associated with the mechanical integrity of the electrode. The active material particles are known undergoing a volume expansion and contraction during lithium insertion and de-insertion processes. The volume change induces severe stress accumulation within thick electrode since the internal stress is hard to release. Therefore, the integrity issue of thicker electrode laminate becomes more severe. The stress accumulation is able to cause the crack or fracture of the electrode laminate [40–42]. Crack appeared within the electrode causes the particle isolation, leading to capacity loss and impedance growth of the electrode. Of course, similar effect also exists in the anode side, which is not subject to investigation in this work.

4. Conclusions

NCM and LFP electrodes of different thicknesses were prepared and investigated. Strong impact of electrode thickness on the rate capability, energy density, power density and long-term cycling behavior is observed. A power–law relation between the active material loading and maximum working *C* rate is developed. The deterioration of rate capability with increasing electrode thickness is mainly due to Li ion diffusion within the electrode. An increase of the internal resistance of the electrode is observed with increasing electrode thickness, which is not the main factor responsible for the significant capacity loss at higher rate for thicker electrode. Energy density of the electrode is improved by increasing the electrode thickness, but at a sacrifice of power density. Long-term cycling behavior of the full cells against MCMB anode shows a higher capacity fading-rate for thicker electrodes. The high capacity fading-rate is ascribed to the severe polarization and mechanical issue of the electrode at higher thickness. Taking all these factors into consideration, in electrode design and fabrication for making lithium ion batteries for EV and PHEV applications, a comprehensive understanding and proper optimization of electrode thickness or active material loading is very critical.

Acknowledgements

The authors are greatly indebted to the funding of Natural Science Foundation of China (NSFC, contract no. 21073129) and the Department of Science and technology of China for the 863 project (2009AA03Z225863).

References

[1] T.J. Patey, A. Hintennach, F.L. Mantia, P. Novák, Journal of Power Sources 189 (1) (2009) 590.
[2] A. Magasinski, P. Dixon, B. Hertzberg, A. Kvit, J. Ayala, G. Yushin, Nature Materials 9 (4) (2010) 353.
[3] I.V. Thorat, D.E. Stephenson, N.A. Zacharias, K. Zaghib, J.N. Harb, D.R. Wheeler, Journal of Power Sources 188 (2) (2009) 592.
[4] K. Zhao, M. Pharr, J.J. Vlassak, Z. Suo, Journal of Applied Physics 108 (2010) 073517.
[5] H. Zheng, G. Liu, X. Song, P. Ridgway, S. Xun, V.S. Battaglia, Journal of the Electrochemical Society 157 (2010) A1060.

[6] Y.H. Chen, C.W. Wang, X. Zhang, A.M. Sastry, Journal of Power Sources 195 (2010) 2851.
[7] H. Zheng, L. Tan, G. Liu, X. Song, V.S. Battaglia, Journal of Power Sources 208 (2012) 52.
[8] I.V. Thorat, V. Mathur, J.N. Harb, D.R. Wheeler, Journal of Power Sources 162 (2006) 673.
[9] G. Liu, H. Zheng, A.S. Simens, A.M. Minor, X. Song, V.S. Battaglia, Journal of the Electrochemical Society 154 (2007) A1129.
[10] G. Liu, H. Zheng, S. Kim, Y. Deng, A.M. Minor, X. Song, V.S. Battaglia, Journal of the Electrochemical Society 155 (12) (2008) A887.
[11] H. Zheng, G. Liu, X. Song, P. Ridgway, S. Xun, V.S. Battaglia, Journal of Physical Chemistry C 116 (7) (2012) 4875.
[12] P. Nelson, I. Bloom, K. Amine, G. Henriksen, Journal of Power Sources 110 (2002) 437.
[13] W. Lu, A. Jansen, D. Dees, P. Nelson, N.R. Veselka, G. Henriksen, Journal of Power Sources 196 (3) (2011) 1537.
[14] M. Doyle, T.F. Fuller, J. Newman, Journal of the Electrochemical Society 140 (1993) 1526.
[15] V. Srinivasan, J. Newman, Journal of the Electrochemical Society 151 (2004) A1517.
[16] M. Wang, J. Li, X. He, H. Wu, C. Wan, Journal of Power Sources 207 (2012) 127.
[17] H. Zheng, G. Liu, X. Song, V. Battaglia, ECS Transactions 11 (32) (2008) 1.
[18] J.W. Fergus, Journal of Power Sources 195 (4) (2010) 939.
[19] W. Zhang, Journal of Power Sources 196 (6) (2011) 2962.
[20] Z. Liu, X. Huang, Solid State Ionics 181 (19-20) (2010) 907.
[21] C. Chang, L. Her, H. Su, S. Hsu, Y. Yen, Journal of the Electrochemical Society 158 (2011) A481.
[22] C.X. Ding, Q.S. Meng, L. Wang, C.H. Chen, Materials Research Bulletin 44 (3) (2009) 492.
[23] J-W. Lee, J-H. Lee, T.T. Viet, J-Y. Lee, J-S. Kim, C-H. Lee, Electrochimica Acta 55 (8) (2010) 3015.
[24] W-M. Chen, L. Qie, L-X. Yuan, S-A. Xia, X-L Hu, W-X. Zhang, Y-H. Huang, Electrochimica Acta 56 (6) (2011) 2689.
[25] B. Huang, X. Zheng, X. Fan, G. Song, M. Lu, Electrochimica Acta 56 (13) (2011) 4865.
[26] M. Dubarry, C. Truchot, M. Cugnet, B.Y. Liaw, K. Gering, S. Sazhin, D. Jamison, C. Michelbacher, Journal of Power Sources 196 (2011) 10328.
[27] M. Dubarry, B.Y. Liaw, Journal of Power Sources 194 (2009) 541.
[28] D.Y.W. Yu, K. Donoue, T. Inoue, M. Fujimoto, S. Fujitani, Journal of the Electrochemical Society 153 (5) (2006) A835.
[29] S.H. Yu, C.K. Park, H. Jang, C.B. Shin, W.I. Cho, Bulletin of the Korean Chemical Society 32 (3) (2011) 852.
[30] Y.S. Chen, K-H. Chang, C-C. Hu, T-T. Cheng, Electrochimica Acta 55 (22) (2010) 6433.
[31] C-K. Park, Z. Zhang, Z. Xua, A. Kakirde, K. Kanga, C. Chai, G. Aub, L. Cristo, Journal of Power Sources 165 (2007) 892.
[32] Y-H. Chen, F-A Li, Journal of Colloid and Interface Science 347 (2010) 277.
[33] T.D. Tran, J.H. Feikert, R.W. Pekala, Journal of Applied Electrochemistry 26 (1996) 1161.
[34] G. Garcia-Belmonte, Electrochemistry Communications 5 (2003) 236.
[35] J. Bisquert, V.S. Vikhrenko, Electrochimica Acta 47 (2002) 3977.
[36] R. Murugaraj, G. Govindaraj, R. Suganthi, D. George, Journal of Material Science 38 (1) (2003) 107.
[37] J. Remmlinger, M. Buchholz, M. Meiler, P. Bernreuter, K. Dietmayer, Journal of Power Sources 196 (2011) 5357.
[38] S.S. Zhang, Journal of Power Sources 161 (2) (2006) 1385.
[39] S.S. Choi, H.S. Lim, Journal of Power Sources 111 (1) (2002) 130.
[40] J. Park, W. Lu, A.M. Sastry, Journal of the Electrochemical Society 158 (2011) A201.
[41] C. Peabody, C.B. Arnold, Journal of Power Sources 196 (19) (2011) 8147.
[42] S. Renganathan, V. Srinivasan, in: 218th ECS Meeting, Abstract #1086, Las Vegas, Nevada, The Electrochemical Society (2010).